# Highly stable Pt-Co bimetallic catalysts prepared by atomic layer deposition for selective hydrogenation of cinnamaldehyde

Kaiying Wang [a], Xiaoqing He [b, c], Jee-Ching Wang [a], Xinhua Liang [a, *]

[a] Linda and Bipin Doshi Department of Chemical and Biochemical Engineering, Missouri University of Science and Technology, Rolla, Missouri 65409, United States

[b] Electron Microscopy Core Facility, University of Missouri, Columbia, Missouri 65211, United States

[c] Department of Mechanical and Aerospace Engineering, University of Missouri, Columbia, Missouri 65211, United States

**Abstract**

Pt-Co bimetallic catalysts were deposited on γ-$Al_2O_3$ nanoparticles by atomic layer deposition (ALD) and were used for selective hydrogenation of cinnamaldehyde (CAL) to cinnamyl alcohol (COL). High resolution transmission electron microscopy, hydrogen temperature-programmed reduction, X-ray diffraction, and X-ray photoelectron spectroscopy were used to identify the strong interaction between Pt and Co. The obtained catalysts with an optimal Pt/Co ratio achieved a COL selectivity of 81.2% with a CAL conversion of 95.2% under mild conditions (i.e., 10 bar $H_2$ and 80 ℃). During the CAL hydrogenation, the addition of Co on Pt significantly improved the activity and selectivity due to the synergetic effects of Pt-Co bimetallic catalysts, resulted from the transfer of electrons from Co to Pt, which can stabilize the carbonyl groups. The obtained Pt-Co bimetallic catalysts also showed excellent stability due to the strong interaction between the metal

nanoparticles and the alumina support. Negligible losses in the activity and selectivity were observed during the recycling experiments, showing the potential for practical applications.

**Key words**: selective hydrogenation; ALD; Pt-Co bimetallic catalysts; stability

## 1. Introduction

Selective hydrogenation is challenging in hydrogenation transformations [1]. Among various catalytic hydrogenation reactions, the selective hydrogenation of α, β-unsaturated carbonyl compounds towards the corresponding unsaturated alcohols plays a critical role, as unsaturated alcohols are important intermediates in fine chemical industries [2-7], such as the production of chemicals, perfume, and pharmaceutical intermediates. Cinnamaldehyde (CAL), a typical α, β-unsaturated carbonyl model compound, is suitable for discriminating the catalytic selectivity between the olefin bond (C=C) or carbonyl group (C=O) hydrogenation. In the hydrogenation of CAL, an intramolecular competition between C=C and C=O exists for reduction with hydrogen. Scheme 1 shows the typical reaction routes of CAL hydrogenation. Compared to C=O, C=C is more prone to be saturated from both thermodynamic (the bond energy is 715 kJ/mol for C=O and 615 kJ/mol for C=C) and kinetic reasons [1]. The key to the selective C=O hydrogenation for forming unsaturated alcohol relies on the fabrication of efficient and selective catalysts.

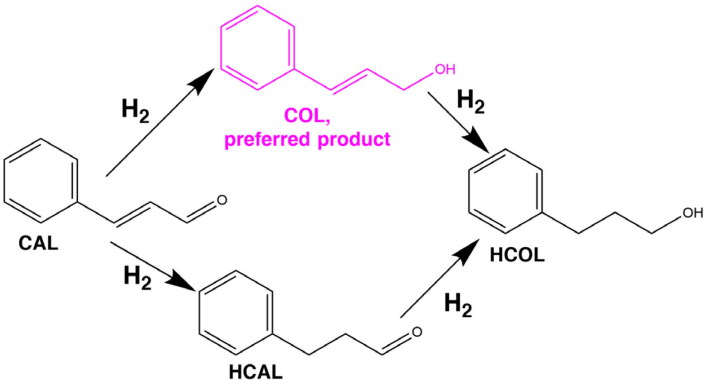


**Scheme 1.** Reaction routes of CAL hydrogenation.

So far, various efforts have been devoted to investigating supported or unsupported group VIII noble metal (e.g., Pt, Pd, Ru, Rh, Os, and Ir) catalysts for CAL hydrogenation [8-10]. As for the selectivity towards unsaturated alcohol, Os and Ir are more selective than Pt, Ru, and Pd, due to larger *d* bands of Os and Ir [11]. Pt based catalysts are preferred because of their relatively lower cost and higher availability than that of Os and Ir. However, unpromoted Pt catalysts usually show low to medium selectivity (<60%) to unsaturated alcohol [12-14]. A variety of strategies have been developed to improve the selectivity of Pt based catalysts, including selective poisoning [15, 16], fabrication of bimetallic catalysts [17, 18], and confinement of nanoparticles (NPs) into porous materials [19]. Generally, the addition of a second metal can improve the selectivity by various electronic and geometric effects. In this respect, the addition of a metal promoter, such as Co [17, 20] or Fe [18], can boost the adsorption of C=O bond in a di-$\sigma_{C=O}$ mode on Pt-based catalysts, thus favoring the hydrogenation of C=O. To date, bimetallic catalysts have been widely used to enhance the selectivity in the hydrogenation of many unsaturated substrates [1, 5-7], such as alkynes, alkenes, imines, and carbonyl compounds. Our previous study has shown that Pt-Co bimetallic catalysts prepared by atomic layer deposition (ALD) can greatly enhance the selectivity of CAL towards C=O hydrogenation, without sacrificing the activity [21].

Catalyst stability is another important issue for practical applications [22]. For example, a decline of CAL conversion from 73% to 64 % was observed after four cycles of CAL hydrogenation experiments over 3.5 wt.%Pt/ graphene catalysts [23]. Zhang et al. employed the identical location TEM (IL-TEM) method [17] to observe the detachment of Pt-Co NPs from carbon nanotube (CNT) support and subsequent NP agglomeration during CAL hydrogenation. Using N-doped CNTs as a support, Su et al. obtained a highly stable Pt-based catalyst due to the strong Pt-N interaction [24]. Huang et. al constructed a sesame cake-like $Pt_3Co$ nanoparticles (NPs)@$Co(OH)_2$ nanosheets (NSs) architecture with strongly coupled $Pt_3Co$−$Co(OH)_2$ interaction for efficient selective hydrogenation catalysis [25]. The obtained catalysts exhibited high stability. Although some progresses have been made in fabricating stable catalysts, the process usually contained toxic materials like ammonia [24], and the synthesis process was too complicated to scale up [25]. It is highly desirable to develop stable catalysts with an environmentally friendly and scalable method. To that end, ALD has been used in this work to prepare a stable PtCo/alumina catalyst with high catalytic activity and selectivity, which is different from previous work that mainly focused on the catalytic activity and selectivity of the catalyst. There is no liquid waste either during the ALD process, and the whole process can be easily scaled up.

In our previous work, the conversion of CAL decreased from 93.4% to 78% and the selectivity toward COL decreased from 93.4% to 75% after three cycles of experiments using 10cCo2cPt/MWCNTs as the catalyst [21]. However, when 5 cycles of $Al_2O_3$ were first deposited on MWCNTs, the obtained 5cCo2cPt/5c-$Al_2O_3$/MWCNTs showed almost the same conversion and selectivity after five cycles of hydrogenation experiments [21]. The interaction of Pt-Co and

$Al_2O_3$ was stronger than that of Pt-Co and MWCNTs. In another work, 30 wt.% of Pt in $Pt/SiO_2$ was lost while only 0.27 wt.% of Pt in $Pt/Al_2O_3$ was lost during a leaching experiment of 72 h in 2-propanol solvent [26]. Therefore, $Al_2O_3$ could be a good support for Pt and Co nanoparticle catalyst. In fact, $Al_2O_3$ is widely used as a support for heterogeneous catalysts in industrial and environmental applications due to its high stability, low cost, and environmental friendliness [27]. Additionally, $\gamma$-$Al_2O_3$ is known to be mildly acidic, and Lewis acidity has been found to promote the polarization and activation of C=O bond [28]. In this study, $Al_2O_3$ was chosen as the support. Pt-Co was deposited on $\gamma$-$Al_2O_3$ NPs by ALD, which is capable of precise control of metal particle size and excellent uniformity [29, 30]. The obtained Pt-Co catalysts on $Al_2O_3$ showed negligible change in the activity and selectivity even after five cycles of experiments.

## 2. Experimental

### 2.1. Chemicals and materials

CAL (99.0%), 2-propanol (99.5%), toluene (99.85% for HPLC), $Co_3O_4$ (99.5%, trace metal basis) and $\gamma$-$Al_2O_3$ (~50 nm) were purchased from MilliporeSigma. Methylcyclopentadienyl)trimethyl platinum [$(MeCp)PtMe_3$] (99%) and cobaltocene ($CoCp_2$, 99%) were obtained from Strem Chemicals, Inc.

### 2.2. Preparation of Pt-Co catalysts

ALD was used to deposit Pt-Co NPs on $\gamma$-$Al_2O_3$ NPs at 300 °C in a fluidized bed reactor. As for Pt ALD, $(MeCp)PtMe_3$ was used as the Pt precursor and oxygen ($O_2$) as the other reactant, as described previously [21]. All solid lines were kept above 120°C to prevent the condensation of any precursors. In a typical run, 3 g of substrates were degassed at 150 °C overnight under nitrogen

($N_2$) atmosphere before ALD. The particle substrates were fully fluidized with the gas flow rates controlled by mass flow controllers. To improve the quality of particle fluidization, the reactor was also subjected to vibration via vibrators. During the Pt ALD process, a solid bubbler containing (MeCp)$PtMe_3$ was heated at 60 °C to achieve a reasonable vapor pressure. The obtained (MeCp)$PtMe_3$ vapor was carried by ultrahigh purity $N_2$ to the reactor. Unreacted precursors and any byproducts were removed by ultrahigh purity $N_2$ during the reaction. The timing sequence for a typical Pt ALD was 180 s, 360 s, 10 s, 180 s, 360 s, and 10 s for (MeCp)$PtMe_3$ dose, $N_2$ purge, evacuation, $O_2$ dose, $N_2$ purge, and evacuation, respectively.

As for Co ALD, $CoCp_2$ and hydrogen ($H_2$) were used as precursors. The reaction was carried out at 300 °C, following the similar procedures as Pt ALD. A solid bubbler containing $CoCp_2$ was heated at 100 °C to obtain high enough vapor pressure. The timing sequence for a typical Co ALD was 180 s, 360 s, 10 s, 180 s, 360 s, and 10 s for $CoCp_2$ dose, $N_2$ purge, evacuation, $H_2$ dose, $N_2$ purge, and evacuation, respectively. In this paper, 2 cycles of Pt were first deposited on γ-$Al_2O_3$ NPs. Then 3, 5, and 8 cycles of Co were deposited on the sample with 2 cycles of Pt ALD. The obtained samples were designated as 2cPt, 3cCo2cPt, 5cCo2cPt, and 8cCo2cPt, respectively. To investigate the performance of monometallic Co, 5 cycles of Co were deposited on γ-$Al_2O_3$ NPs, denoted as 5cCo. To investigate the different behaviors of unsupported samples from those supported ones, 1 cycle of Pt was deposited on $Co_3O_4$ particles. The process was the same as Pt ALD on γ-$Al_2O_3$. The obtained unsupported catalyst was denoted as 1cPt-$Co_3O_4$.

### 2.3. Catalyst characterizations

To evaluate the crystalline structure and particle size of both Pt and Co NPs, high resolution TEM was conducted by using a ThermoFisher Scientific Tecnai G2 FEG F30 microscope operated at 300 keV. Scanning TEM (STEM) high angle annular dark field images were used to highlight the contrast of the Pt and Co NPs from the $Al_2O_3$ substrate. The STEM-energy dispersive X-ray spectroscopy (EDS) was performed to confirm element species using a Bruker Quantax 400 EDS. The electron energy loss spectroscopy (EELS) in the energy filtered TEM mode was used to confirm the presence of Co using a Gatan Quantum image filter. X-ray diffraction (XRD) measurements were performed using a Philips X'Pert PRO PW3050 X-ray diffractometer, equipped with a Cu Kα radiation and a graphite generator, in a 2θ range of 10–90° to obtain crystal structure of catalysts.

Pt and Co mass contents were obtained by inductively coupled plasma - optical emission spectrometry (ICP-OES). The samples were digested with the assistance of a Titan MPS microwave digestion system. X-ray photoelectron spectroscopy (XPS) analysis was performed to verify the formation of bimetallic structure of Pt-Co catalysts. XPS spectra of Pt, Co, and Pt-Co catalysts were recorded with a Kratos Axis 165 X-ray photoelectron spectrometer using a monochromatic Al Ka radiation. All binding energy values were corrected to C 1s signal (284.6 eV).

$H_2$ temperature-programmed reduction ($H_2$-TPR) was examined by employing 150 mg sample in each measurement, using Micromeritics Autochem II 2920 equipped with a thermal conductivity detector (TCD). First, the sample was pretreated by Ar at 350 °C for 1 h (heating rate of 10 °C/min).

Then, the temperature was cooled down to room temperature in an Ar flow with a flow rate of 30 mL/min. Finally, the temperature was ramped up to 900 °C at 10 °C /min under 10% $H_2$ in Ar flow.

### 2.4. Hydrogenation of CAL

All catalysts were reduced under $H_2$ at 300°C for 2 h prior to reactions. Then, the catalysts were cooled down to room temperature under $N_2$. Certain amount of the catalysts was transferred to a 50 mL stainless steel Parr reactor, containing 0.5 g CAL as well as 30 mL 2-propanol. After that, the reactor was flushed with 10 bar $H_2$ 6 times to repel air out of the reactor at room temperature. Then, the reactor was pressurized with $H_2$ to a desired value (5,10, 20, and 30 bar). Reaction was conducted at 80 °C for 9 h while stirring at a speed of 800 rpm to eliminate mass transfer resistance [21]. During the reaction, around 1 mL of sample was withdrawn periodically and quantified by a gas chromatography (GC, Agilent 6890), with toluene as an internal standard. For the cycling experiments, the catalysts were washed with 2-propanol for three times and collected by centrifugation.

## 3. Results and discussions

### 3.1. Characterizations of Pt-Co catalysts

TEM images of the Pt and Pt-Co catalysts are shown in Fig.1. Pt NPs and Pt-Co NPs have narrow size distributions with a size range of 1.1 to 1.4 nm and 1.4 to 1.7 nm, respectively. The crystal fringes can be easily observed in the lower inset of Fig. 1a, where the *d*-spacing was measured to be 0.228 nm, which matches well with the (1 1 1) planes of the face-centered cubic Pt crystals. As for the Pt-Co samples, EELS was used first to locate a region where Co was present, as shown in Fig. S1a. The average size of the Pt-Co bimetallic NPs increased to 2.1 nm and the size distribution

was broader. Figure1b is a typical HRTEM image of the bimetallic Pt-Co particles where the inset clearly showed high crystallinity of both particles and their being close to each other. Measurement of the lattice spacings confirmed the existence of both Pt and hexagonal Co. The hexagonal Co particle can be unambiguously identified matching the measured d spacing measures of (0001) and (0110) with the hexagonal Co structure in the Inorganic Crystal Structure Database (ICSD_52935), which can been seen in the lower inset of Fig.1b. To further confirm the presence of Pt and Co, the localized scanning on the two particles shown in the inset clearly showed the Co and Pt peaks in the EDS spectrum in Fig. S1b. To this end, our TEM data clearly identified both Co and Pt being close together and forming so-called "bimetallic" NPs. Pt and Pt-Co NPs were highly dispersed on $\gamma$-$Al_2O_3$ in all samples, as shown in Figs. S1c and S1d. XRD measurements were performed to study the crystal structure of the catalysts. As can be seen from Fig. S2, the peaks for Pt were hardly detected because of its high dispersion and small particle size [31, 32]. As for the reflections of Co, only broad peaks were observed, which were coincident with those of the $\gamma$-$Al_2O_3$ support [33]. The XRD analysis also confirmed the high dispersion of Pt-Co NPs.

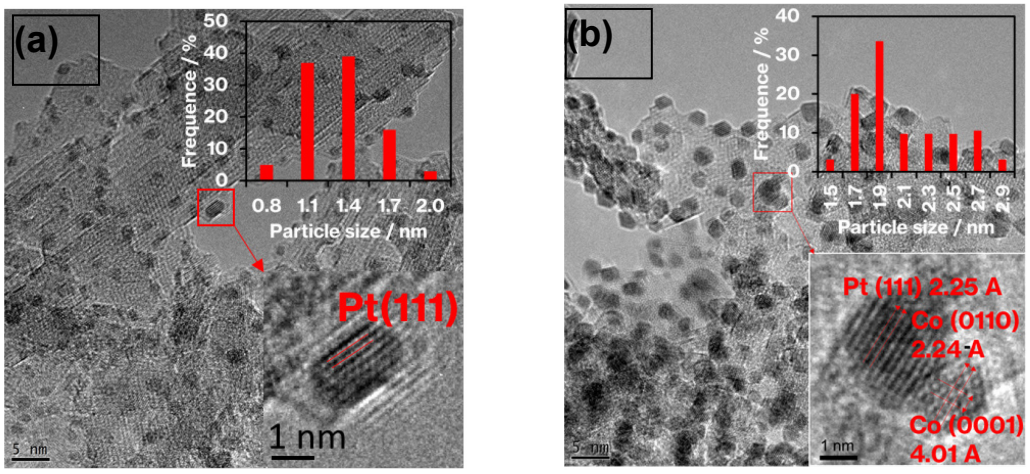


**Fig. 1** HRTEM images of (a) 2cPt sample and (b) 5cCo2cPt sample.

The bulk metal content was obtained by ICP-OES, and the results are shown in Table 1. Pt content was 5.24% in the 2cPt sample, and it decreased as Co was deposited. The surface electronic properties of Pt in different Pt-based catalysts were analyzed by XPS. As Pt 4f region was overlapped by the strong Al 2p peak, Pt 4d region was used to analyze the surface Pt compositions of the catalysts. Figure 2 shows Pt 4d spectra of 2cPt, 3cCo2cPt, 5cCo2cPt, and 8cCo2cPt samples, together with their deconvolution obtained by the Gaussian-Lorentzian method after Shirley-background subtraction. The Pt 4d spectra of the 2cPt sample clearly demonstrated the presence of two different chemical environments of Pt atoms with Pt $4d_{5/2}$ at 314.3 eV and 320.8 eV, which are attributed to $Pt^0$ and $Pt^{2+}$, respectively [34]. The presence of $Pt^{2+}$ indicates that some Pt atoms were oxidized in the air after the Pt ALD process. The fraction of metallic $Pt^0$ increased progressively from the mono-metallic 2cPt (83.25%) sample to the 3cCo2cPt (84.12%) and 5cCo2cPt (84.36%) samples. Thus, the addition of appropriate Co amounts enhanced the reduction of $Pt^{2+}$, which is consistent with a previous study [35]. Fu et al. also confirmed that metallic Pt preferred the adsorption of C=O [23]. The binding energy (BE) of $Pt^0$ in 2cPt slightly shifted from 314.3 eV to 314.2 eV, when 5 cycles of Co ALD were deposited on the Pt/alumina sample. It further shifted to 313.4 eV, when 8 cycles of Co ALD were applied. Such a trend indicates that the *d* band center of Pt–Co bimetallic nanostructures caused BE downshifts [36, 37]. It is known that BE is strongly correlated with the adsorption/desorption capability of reaction species on the catalyst surface. The lower BE in 5cCo2cPt (314.2 eV) indicates a higher electron density around Pt, mainly caused by the charge transfer from Co to Pt. The higher electron density of surface Pt in 5cCo2cPt would result in stronger repulsion against C=C, hindering the hydrogenation of the C=C bond [38]. Furthermore, as more Co was deposited, the surface Pt/Co molar ratio decreased,

from 0.42 in 3cCo2cPt to 0.30 when 5 cycles of Co ALD were deposited and further down to 0.12 when 8 cycles of Co ALD were applied. The Pt/Co molar ratio plays a critical role in the catalytic performance, which will be discussed in detail in the following section.

**Table 1.** Pt and Co bulk content and surface composition.

| Sample | Pt, wt.% | Co, wt.% | Pt/Co bulk molar ratio [a] | Pt/Co surface molar ratio [b] | Fraction of $Pt^0$ [c], % |
|---|---|---|---|---|---|
| 5cCo | - | 4.06 | - | - | - |
| 2cPt | 5.24 | - | - | - | 83.25 |
| 3cCo2cPt | 4.93 | 2.59 | 0.58 | 0.42 | 84.12 |
| 5cCo2cPt | 4.40 | 3.49 | 0.38 | 0.30 | 84.36 |
| 8cCo2cPt | 3.79 | 7.59 | 0.15 | 0.12 | 76.35 |
| 5cCo2cPt[d] | 4.32 | 3.38 | 0.39 | 0.31 | 83.86 |

a. Pt/Co bulk molar ratio obtained from ICP-OES.
b. Pt/Co surface molar ratio obtained from XPS survey scan.
c. Fraction of $Pt^0$ obtained from deconvolution of Pt 4d spectra.
d. 5cCo2cPt after five cycles of hydrogenation experiment.

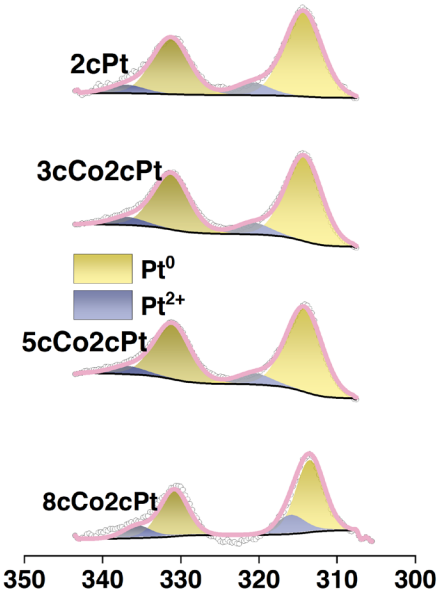


**Fig. 2** Pt 4d XPS spectra of 2cPt, 3cCo2cPt, 5cCo2cPt, and 8cCo2cPt.

$H_2$-TPR experiments were carried out to investigate the reducibility of the samples. The $H_2$-TPR profiles are displayed in Fig. 3. γ-$Al_2O_3$ did not consume $H_2$ in the analyzed temperature range (100-900°C), as shown in Fig. 3b. PtO species were easily reduced to $Pt^0$ below 100 °C, consistent with previous reports [39, 40]. The unsupported $Co_3O_4$ started to be reduced at 200 °C, and it was fully reduced at around 580 °C. The supported 5cCo sample showed a different behavior. As shown in Fig. 3a, the reduction peak at 520 °C was ascribed to $Co^{3+} \rightarrow Co^{2+}$, and the peak at 630 °C came from $Co^{2+} \rightarrow Co^0$ reduction [41]. The peak at 850 °C correlated to the reduction of Co ions in cobalt aluminate ($CoAl_2O_4$) [40]. Higher reduction temperature for the Co/alumina samples can be ascribed to the strong interaction between $Al_2O_3$ and Co [41, 42]. Regarding the Pt-Co bimetallic catalysts, the reduction of cobalt oxide occurred at a lower temperature. Previous research pointed out that Pt could boost the reduction of cobalt oxide markedly [41], because the presence of Pt promoted dissociation and activation of hydrogen. As can be see from Fig.3b, for

the unsupported 1cPt-$Co_3O_4$ sample, the peak temperature of $Co^{3+}$ to $Co^{2+}$ reduction greatly reduced from 320 °C to 220 °C, and the peak temperature of $Co^{2+}$ to $Co^0$ reduction reduced from 460 °C to 340 °C. As for the supported 8cCo2cPt sample, the reduction peak can be deconvoluted to two peaks, 370°C for $Co^{3+}$ to $Co^{2+}$ reduction peak, and 540°C for $Co^{2+}$ to $Co^0$ reduction peak, respectively. The reduction temperature for the supported 8cCo2cPt sample was 150°C higher than that of the unsupported 1cPt-$Co_3O_4$ sample, indicating strong metal-support interaction. The interaction between the cobalt ions and the support notably hindered both reduction steps, $Co^{3+}$ to $Co^{2+}$ and $Co^{2+}$ to $Co^0$. Therefore, the $H_2$-TPR analysis further confirmed the structure of Pt-Co bimetallic NPs, which was consistent with the XPS results.

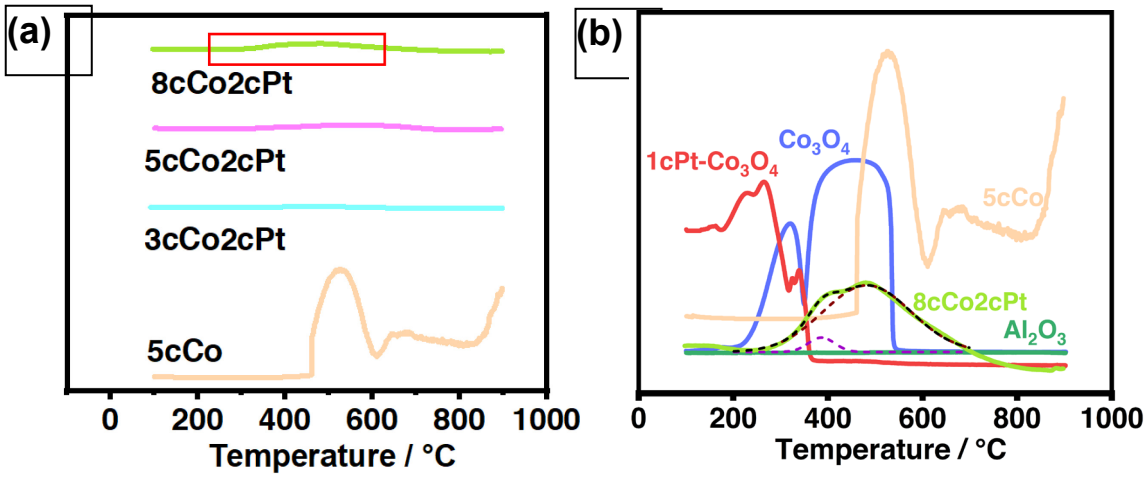


**Fig. 3** $H_2$-TPR profiles of (a) prepared Pt-Co catalysts, and (b) supported (i.e., 5cCo and 8cCo2cPt) and unsupported (i.e., $Co_3O_4$ and 1cPt-$Co_3O_4$) Co and Pt-Co samples.

### 3.2. Catalytic performance

#### 3.2.1. Effects of Pt/Co ratios

The effects of Pt/Co ratios on CAL conversion and COL selectivity were investigated. For comparison, both Pt only sample and Co only sample were also tested. As shown in Fig. 4, the Pt only sample exhibited the lowest COL selectivity. The Co only sample showed a high COL selectivity, but a low CAL conversion of only 25.6% after 9 h of reaction, which was consistent with our previous work [21]. When 3 cycles of Co ALD were applied on the 2cPt sample, both of the conversion and selectivity were higher than those of the Pt only sample. When more Co was deposited using 5 cycles of ALD, the obtained 5cCo2cPt sample exhibited the highest CAL conversion and COL selectivity. A detailed CAL conversion and COL selectivity as a function of reaction time can be found in Fig. S3.

The significant enhancements in the CAL conversion and the COL selectivity provided by Pt-Co bimetallic catalysts can be ascribed to the synergistic effects between Pt and Co, rather than those of Co individually, since the Co monometallic catalyst showed the lowest CAL conversion. More specifically, the enhancements seen in the case of 3cCo2cPt and 5cCo2cPt samples can be contributed to the $H_2$ spillover effect of Pt, as confirmed by $H_2$-TPR presented above. However, when 8 cycles of Co ALD were applied, the selectivity to COL almost remained unchanged, but the conversion of CAL decreased from 95.2% to 47.9%. This was consistent with its XPS results where its Pt/Co surface molar ratio dropped to 0.12, meaning that most of Pt NPs in this case could be covered by Co NPs, causing low activity. Therefore, the 5cCo2cPt sample was used in the following experiments.

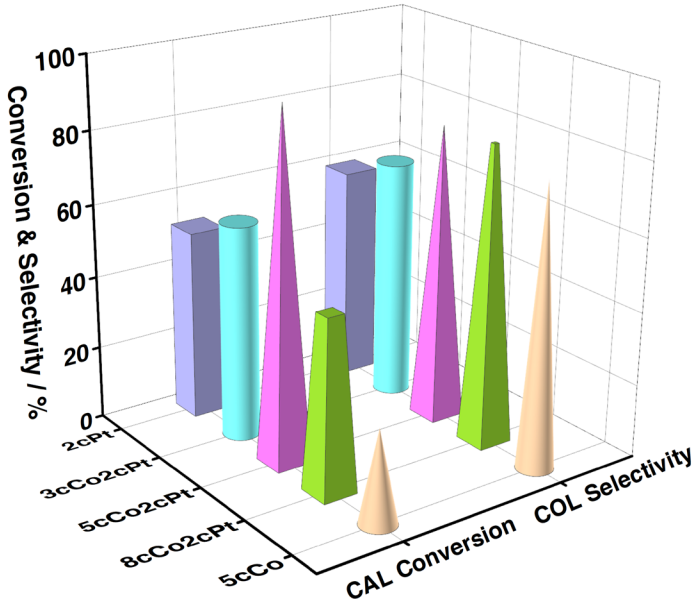


**Fig. 4** Effects of Pt/Co ratios on CAL conversion and COL selectivity.

### 3.2.2 Effects of catalyst dosage

The effects of catalyst dosage on CAL conversion and COL selectivity were also investigated. For this purpose, the most desirable 5cCo2cPt catalyst was used and the results are shown in Fig.5.

With the increase of catalyst dosage, CAL conversion increased significantly. CAL was 100% consumed in 6 h when 20 mg of 5cCo2cPt was added. When 10 mg of 5cCo2cPt was added, 95.2% of CAL was reacted in 9 h. However, only 64.1% of CAL was consumed when 5 mg of 5cCo2cPt was added. As for the selectivity, 80% of COL selectivity was achieved in 1.25 h in the case of 20 mg of 5cCo2cPt. The selectivity of COL dropped as the reaction continued. That could be resulted from further hydrogenation COL to HCOL, since 85% of CAL was already consumed in 1.25 h. When the catalyst dosage reduced to 5 mg and 10 mg, the selectivity of COL increased as the reaction continued. 10 mg of 5cCo2cPt exhibited the highest COL selectivity of 81.2% with 95.2% CAL conversion. Thus, in the following experiments, 10 mg of catalysts was used.

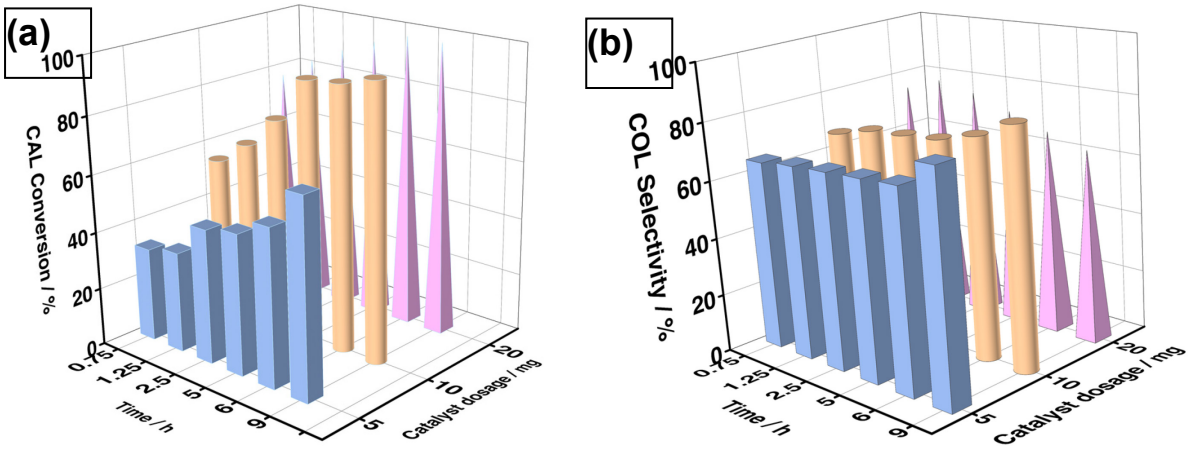


**Fig. 5** Effects of catalyst dosage on (a) CAL conversion and (b) COL selectivity over the 5cCo2cPt catalyst.

### 3.2.3. Effects of reaction pressure

The impact of hydrogen pressure upon CAL hydrogenation was investigated over 10 mg of the most active 5cCo2cPt catalyst under various hydrogen pressure (i.e., 5, 10, 20, and 30 bar) at 80 °C. In general, higher hydrogen pressure increases the availability of molecular hydrogen in the solvents due to higher solubility. The increased hydrogen in the solvents improves the mass

transfer, thereby enhancing the adsorption of hydrogen on the active sites. Typically, liquid phase hydrogenations show positive reaction order with respect to the hydrogen partial pressure. As expected, increasing the hydrogen pressure boosted the conversion as soon as the reaction started, which is clearly shown in Fig.6. Similar trends have been reported in many liquid hydrogenation reactions in the literature [43-45]. For example, steady increases of CAL conversion from 21.6% at 1.5 bar to 83% at 10 bar and to a plateau value at about 20 bar were observed over unsupported Pt-based nanocrystals [45]. These conversion increases have been ascribed to enhanced mass transfer under higher pressure [46]. The pressure also has a great effect on the selectivity of COL. As shown in Fig.6, the selectivity of COL dropped from 82.4% to 46.4% when the pressure increased from 5 bar to 30 bar. This is because, as the pressure increased, the hydrogenation of both C=O and C=C proceeded further along to form HCOL [47]. Similar trends can also be found in some previous studies [47-49]. Nevertheless, the influence of hydrogen pressure on the selectivity of COL is still under debate. For instance, Lee et al. observed an enhanced selectivity towards COL when 2% Pt/SBA-15 was used as the catalysts and the hydrogen pressure increased from 1 bar to 10 bar [43]. The cause of different selectivity changes due to $H_2$ pressure remains unresolved to date. One possible explanation is the switchover from Pt (111) to Pt (100) facets induced by high hydrogen pressure, which was confirmed by Cuenya et al. through *in situ* X-ray absorption near-edge structure (XANES) analysis upon Pt/$\gamma$-$Al_2O_3$ NPs [44]. Based on Delbecq and Sautet's research finding that Pt (111) favored a di-$\delta_{CO}$ $\eta_2$ adsorption, while Pt (100) favored a co-planar $\eta_4$ adsorption [50], more Pt (100) facets were exposed under higher pressure, hence increasing C=C hydrogenation and lowering the selectivity towards COL.

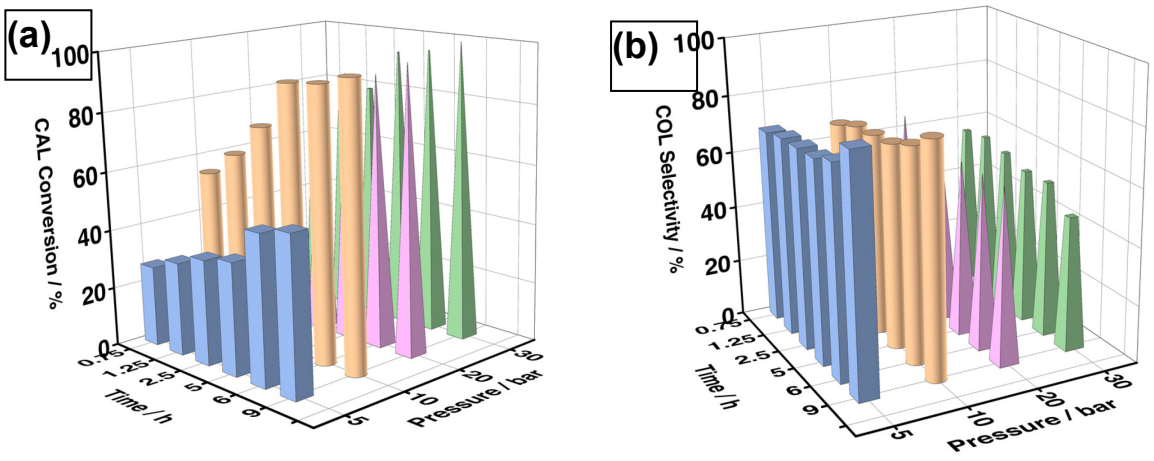


**Fig. 6** Hydrogen pressure dependence of (a) CAL conversion and (b) COL selectivity over 5cCo2cPt catalysts.

### 3.2.4. Stability of the catalysts

Catalyst stability is a very important factor in their practical applications. For this reason, the stability of the most promising 5cCo2cPt catalyst for CAL hydrogenation was further studied. After each reaction run, the catalyst was washed three times with 2-propanol and collected by centrifugation. The obtained catalysts were then used for the next run under the same reaction conditions. As shown in Fig.7, the conversion of CAL and the selectivity toward COL exhibited only negligible decreases, indicating excellent stability of the 5cCo2cPt catalyst. In addition, the surface Pt/Co molar ratio of the used catalyst based on XPS analysis was 0.31, which was very close to 0.30 for the fresh 5cCo2cPt catalyst. Its bulk content of Pt and Co also decreased very slightly according to the ICP-OES results listed in Table 1. The excellent stability of the catalyst can be attributed to the strong interaction between the support and the Pt-Co NPs. As confirmed by $H_2$-TPR in Fig.3b, the reduction temperature of the supported PtCo samples can be 150 °C higher than the unsupported ones. In particular, the formation of cobalt aluminate spinel greatly

improved the stability. By fulfilling this essential need, the catalyst can be expected to be very potential for the practical applications.

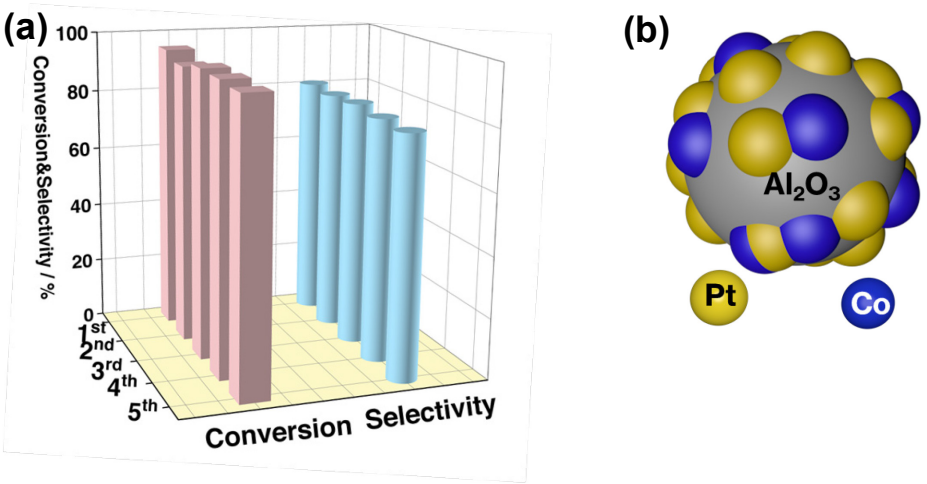


**Fig. 7** (a) Stability test of CAL hydrogenation over the 5cCo2cPt catalyst, and (b) schematic representation for the formation of cobalt aluminate spinel that improves the catalyst stability.

### 3.2.5. Discussions

Based on the results and comparisons presented above, the increase of selectivity to COL is due to the change of the electronic structure of Pt atoms upon Co deposition. It is an effective way to improve the selectivity to the desired products by using bimetallic Pt-based catalysts. Correspondingly, Fe or Co is often doped with Pt to facilitate C=O hydrogenation while Ni is often doped with Pt to be favorable for C=C hydrogenation. This variation in selectivity is due to the difference in their d-band center position from the Fermi level when the Pt nanocrystal surface is electronically modified by the transition metal [45]. As d-band center moves close to the Fermi level, a stronger and more thermodynamically favorable di-σ metal C–C bond is preferred over di-σ metal C–O on NiPt and Pt surfaces, which reduces the selectivity of the hydrogenation of the C=O bond. As the d-band center moves away from the Fermi level, the di-σ metal C–C binding energy decreases, thus leading to a more selective C=O hydrogenation pathway. Thus, the

selectivity is maximized at around FePt and CoPt, which indicate that the position of the d-band center on these surfaces corresponds with the optimal binding energy of C=O in cinnamaldehyde. The relationship between the selectivity to cinnamyl alcohol with respect to the position of d-band center of the 1st row transition doper metal referenced to its Fermi level can be found in the reference[45].

The above-mentioned d-band theory has also been validated by experiments. For example, an 88.2% selectivity of HCAL was obtained by using carbon nanotubes supported Pt–Ni catalysts [51]. In a recent study, the selective hydrogenation of C=O and C=C can be adjusted by varying the Ni/Fe ratios [48]. A 92.2% COL selectivity was achieved on $Pt/FeAl_2O_4$. Instead, an 80.7% HCAL selectivity was obtained on $Pt/NiAl_2O_4$. Moreover, Qin et al. demonstrated that ALD deposited Fe could selectively block low coordination Pt sites, which favored π interactions with C=C bond [18]. Tsang et al. also found that Co atoms could selectively block low coordination Pt sites to greatly improve the selectivity to COL [52]. In our previous work, a 93.3% COL selectivity was obtained by carbon nanotubes supported Pt–Co catalysts [21].

In this work, Co deposited by ALD could also selectively block low coordinated Pt sites to increasing the selectivity to C=O bond. As confirmed by the XPS results, the bimetallic Pt-Co catalysts facilitated the electron transfer from Co to Pt, synergistically enhancing the selectivity to COL. Besides, the addition of Co also greatly enhanced the catalytic activity. To be more insightful, mass-specific rates of CAL consumption ($MSA_{CAL}$) and COL formation ($MSA_{COL}$) were normalized based on per gram of Pt per hour. As shown in Fig. 8, both $MSA_{CAL}$ and $MSA_{COL}$ exhibited a volcano-like shape as the Co increased. The $MSA_{CAL}$ increased from 1.31 $mol_{CAL}\cdot g_{Pt}\cdot h^{-1}$ for the 2cPt sample to 7.14 $mol_{CAL}\cdot g_{Pt}\cdot h^{-1}$ for the 3cCo2cPt sample. The highest $MSA_{CAL}$

achieved was equal to 16.13 $mol_{CAL} \cdot g_{Pt} \cdot h^{-1}$ for the 5cCo2cPt sample, which represents a 12-fold increase over that of the 2cPt sample without any Co. However, the $MSA_{CAL}$ decreased to 5.02 $mol_{CAL} \cdot g_{Pt} \cdot h^{-1}$ by further increasing Co content to 8cCo2cPt. The highest $MSA_{COL}$ was also obtained for the optimal 5cCo2cPt catalyst, at 11.55 $mol_{COL} \cdot g_{Pt} \cdot h^{-1}$, which corresponds to 81.17% COL selectivity. Similar results have been reported in a previous study using PtFe catalysts, where the $MSA_{CAL}$ was increased almost 13 times by the optimal $PtFe_{0.25}$ sample [53].

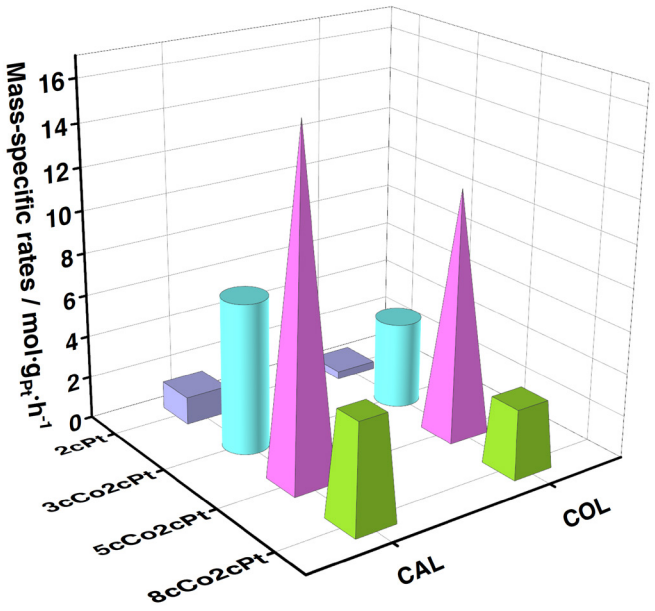


**Fig. 8** $MSA_{CAL}$ and $MSA_{COL}$ of catalysts with different Pt/Co ratios.

To further elucidate the enhanced selectivity to COL by adding Co to Pt, the hydrogenation of a mixture containing equivalent semi-hydrogenated products, such as HCAL (only containing C=O double bond) and COL (only containing C=C double bond), was investigated on the 2cPt and 5cCo2cPt samples. The product distribution is shown in Fig. 9. For the 2cPt sample, COL was consumed faster than HCAL, indicating that C=C hydrogenation was preferred on 2cPt. The correlation between $\ln(C_0/C_t)$ and reaction time (t) was made to evaluate the kinetic behaviors. $C_0$ represents the initial molar concentration of COL or HCAL, while $C_t$ represents the molar

concentration of COL or HCAL that varies with reaction time. As can be seen from Fig. 9c, COL and HCAL hydrogenation showed a liner correlation between $\ln(C_0/C_t)$ and reaction time (t), confirming the 1st order reaction of COL and HCAL hydrogenation. The rate constant $k$ was obtained according to the equation $\ln(C_0/C_t) = kt$. The $k_{C=C}$ of COL hydrogenation was 6.1 x $10^{-3}$ $min^{-1}$, and the $k_{C=O}$ of HCAL hydrogenation was 1.9 x $10^{-3}$ $min^{-1}$, respectively. The COL and HCAL hydrogenation on 5cCo2cPt also followed the 1st order reaction. The $k_{C=C}$ of COL hydrogenation was 8 x $10^{-4}$ $min^{-1}$, and the $k_{C=O}$ of HCAL hydrogenation was 5.8 x $10^{-3}$ $min^{-1}$, respectively. Accordingly, $k_{C=O}/ k_{C=C}$ ratio of 5cCo2cPt was 7.25, which was higher than that of 2cPt (0.31).

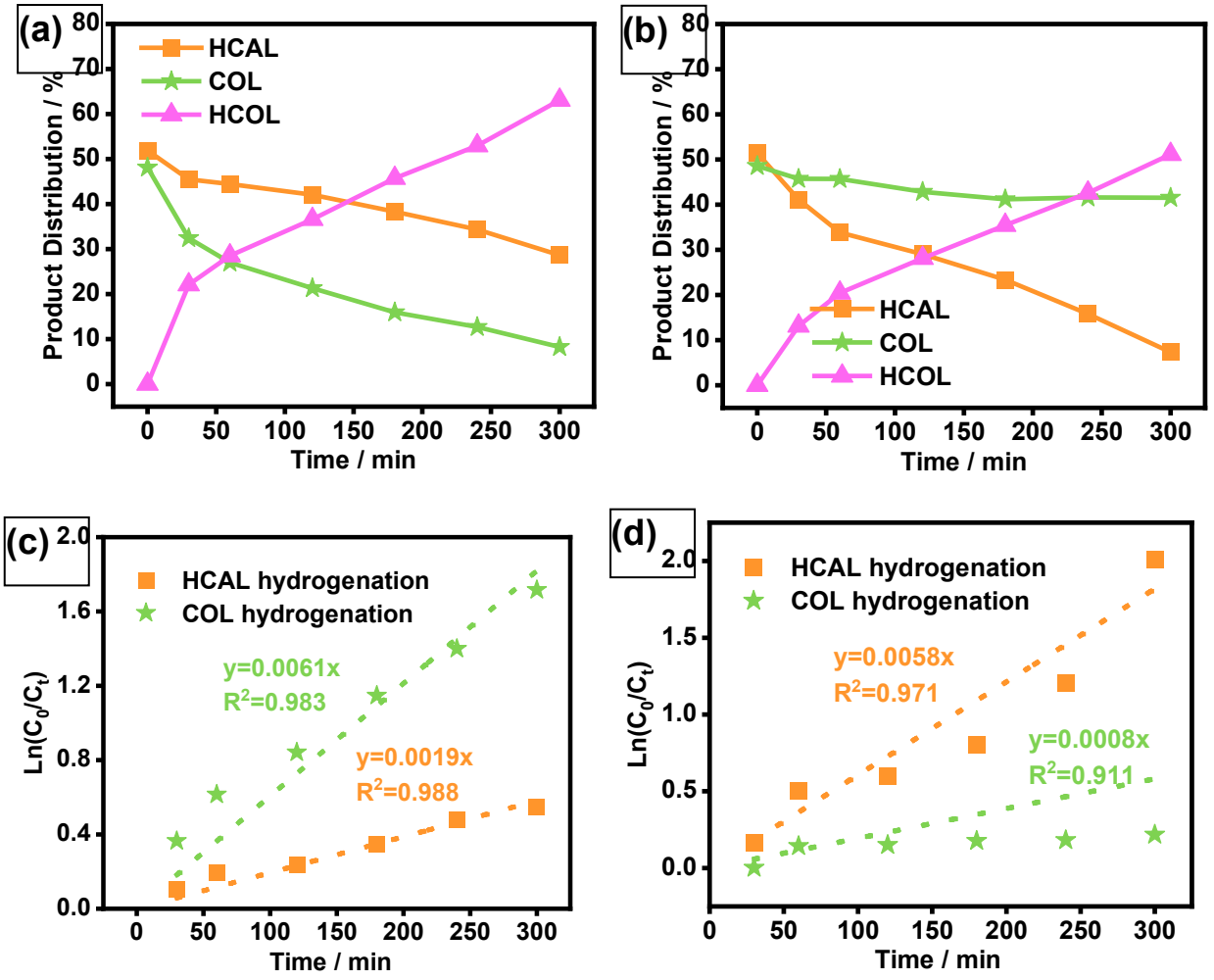


**Fig. 9** Production distribution of the hydrogenation of COL and HCAL on (a) 2cPt, and (b)5cCo2cPt samples; $\ln(C_0/C_t)$ *vs* time for the hydrogenation of COL and HCAL on (c) 2cPt, and (d) 5cCo2cPt samples.

Therefore, the addition of a second metal promoter and the strong interactions between the support and the metals can be an effective strategy to improve the performance and stability. To evaluate the universality of this strategy, 1 cycle of Co ALD was deposited on $Pt/SiO_2$ sample prepared by ALD, and the obtained catalyst was used for CAL hydrogenation. As shown in Fig. S4, CAL conversion increased from 38.0% to 71.9% when Co was added to the $Pt/SiO_2$ sample. COL selectivity also greatly enhanced from 47.3% to 77.9%. However, $PtCo/SiO_2$ was unstable in liquid

phase, due to the weak interaction between the metal NPs and the support. Finally, a possible reaction pathway can be proposed as shown in Scheme 2. Monometallic Pt sample showed lower selectivity to COL, since it favored C=C adsorption and hence hydrogenation over C=C was easier than C=O. The addition of Co changed the electronic state of the Pt, thus changing the CAL adsorption preference towards di-$\delta_{CO}$ $\eta_2$ adsorption, which led to C=O hydrogenation, thus improving the selectivity of COL. Moreover, Co also contributed to the catalytic activity, due to the hydrogen spillover effect from Pt. Therefore, the optimized Pt-Co bimetallic catalysts exhibited both higher activity and selectivity than that of monometallic samples. The strong interactions between the support and the metal boosted the stability remarkably.

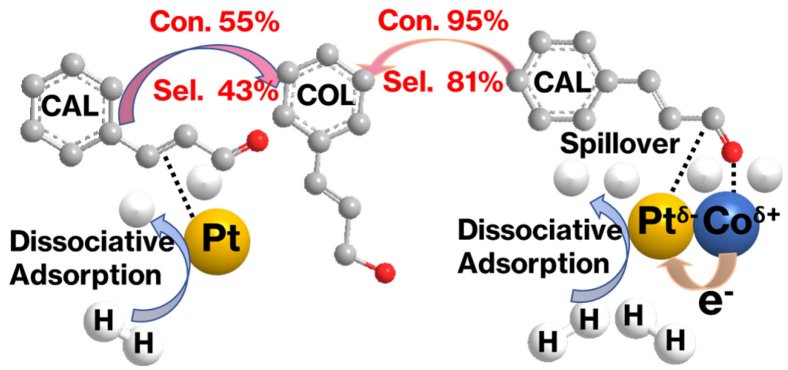


**Scheme 2.** A possible reaction pathway of CAL hydrogenation.

## Conclusions

In summary, a series of highly dispersed Pt-Co bimetallic nanoparticles supported on $Al_2O_3$ with different Pt/Co ratios were prepared by ALD. An optimal 5cCo2cPt catalyst exhibited the best catalytic performance in CAL hydrogenation, achieving 81.2% COL selectivity with 95.2% CAL conversion. The improvement of catalytic performance can be ascribed to the addition of Co, which changed the electronic state of Pt and enhanced the selectivity to COL notably. The synergistic effects of Pt and Co were verified through various characterization techniques.

Moreover, the synthesized catalyst showed excellent stability, which is essential for practical applications. The bimetallic strategy built on the synergetic effects presented in this work can be not only applied to other metal nanoparticles and supports, but also regarded as a universally rational approach for designing and synthesizing effective catalysts for selective hydrogenation reactions. The research findings from this work concerning the catalyst-support interaction can also be incorporated into future studies aimed at the stability issue that still exists in many other catalyst supports.

## Conflicts of interest

There are no conflicts to declare.


## Acknowledgements

This work was supported by the National Science Foundation grant NSF 1803812.

## References


[1] Zhang L, Zhou M, Wang A and Zhang T 2020 Selective Hydrogenation over Supported Metal Catalysts: From Nanoparticles to Single Atoms *Chem. Rev.* **120** 683-733

[2] Zugic B, Karakalos S, Stowers K J, Biener M M, Biener J, Madix R J and Friend C M 2016 Continuous Catalytic Production of Methyl Acrylates from Unsaturated Alcohols by Gold: The Strong Effect of C═C Unsaturation on Reaction Selectivity *ACS Catal.* **6** 1833-9

[3] Smith K K, Redeker N D, Rios J C, Mecklenburg M H, Marcischak J C, Guenthner A J and Ghiassi K B 2019 Surface Modification and Functionalization of Boron Nitride Nanotubes via Condensation with Saturated and Unsaturated Alcohols for High Performance Polymer Composites *ACS Appl. Nano Mater.* **2** 4053-60

[4] Xu J, Sun J, Zhao J, Huang B, Li X and Sun Y 2017 Palladium-Catalyzed Synthesis of Quinolines from Allyl Alcohols and Anilines *RSC Adv.* **7** 36242-5

[5] Wang X, Liang X, Geng P and Li Q 2020 Recent Advances in Selective Hydrogenation of Cinnamaldehyde over Supported Metal-Based Catalysts *ACS Catal.* **10** 2395-412

[6] Luneau M, Lim J S, Patel D A, Sykes E C H, Friend C M and Sautet P 2020 Guidelines to Achieving High Selectivity for the Hydrogenation of alpha,beta-Unsaturated Aldehydes with Bimetallic and Dilute Alloy Catalysts: A Review *Chem. Rev.* **120** 12834-72

[7] Lan X and Wang T 2020 Highly Selective Catalysts for the Hydrogenation of Unsaturated Aldehydes: A Review *ACS Catal.* **10** 2764-90

[8] Geng F, Bonita Y, Jain V, Magiera M, Rai N and Hicks J C 2020 Bimetallic Ru–Mo Phosphide Catalysts for the Hydrogenation of $CO_2$ to Methanol *Ind. Eng. Chem. Res.* **59** 6931-43

[9] Bonita Y, Jain V, Geng F, O'Connell T P, Ramos N X, Rai N and Hicks J C 2020 Hydrogenation of Cinnamaldehyde to Cinnamyl Alcohol with Metal Phosphides: Catalytic Consequences of Product and Pyridine Doping *Appl. Catal. B* **277** 119272-82

[10] Yuan K, Song T, Wang D, Zhang X, Gao X, Zou Y, Dong H, Tang Z and Hu W 2018 Effective and Selective Catalysts for Cinnamaldehyde Hydrogenation: Hydrophobic Hybrids of Metal-Organic Frameworks, Metal Nanoparticles, and Micro- and Mesoporous Polymers *Angew. Chem. Int. Ed.* **130** 5810-5

[11] Gallezot P and Richard D 1998 Selective Hydrogenation of α,β-Unsaturated Aldehydes *Catal. Rev. - Sci. Eng.* **40** 81-126

[12] Szöllösi G, Török B, Szakonyi G, Kun I and Bartók M 1998 Ultrasonic Irradiation as Activity and Selectivity Improving Factor in the Hydrogenation of Cinnamaldehyde over $Pt/SiO_2$ Catalysts *Appl. Catal. A* **172** 225-32

[13] Lashdaf M, Nieminen V-V, Tiitta M, Venäläinen T, Österholm H and Krause O 2004 Role of Acidity in Hydrogenation of Cinnamaldehyde on Platinum beta Zeolite *Microporous Mesoporous Mater.* **75** 149-58

[14] Handjani S, Marceau E, Blanchard J, Krafft J-M, Che M, Mäki-Arvela P, Kumar N, Wärnå J and Murzin D Y 2011 Influence of the Support Composition and Acidity on the Catalytic Properties of Mesoporous SBA-15, Al-SBA-15, and $Al_2O_3$-Supported Pt Catalysts for Cinnamaldehyde Hydrogenation *J. Catal.* **282** 228-36

[15] Liu H, Mei Q, Li S, Yang Y, Wang Y, Liu H, Zheng L, An P, Zhang J and Han B 2018 Selective Hydrogenation of Unsaturated Aldehydes over Pt Nanoparticles Promoted by the Cooperation of Steric and Electronic Effects *Chem. Commun.* **54** 908-11

[16] Gao R, Pan L, Wang H, Yao Y, Zhang X, Wang L and Zou J J 2019 Breaking Trade-Off between Selectivity and Activity of Nickel-Based Hydrogenation Catalysts by Tuning Both Steric Effect and d-Band Center *Adv. Sci.* **6** 1900054

[17] Su J, Shi W, Liu X, Zhang L, Cheng S, Zhang Y, Botton G A and Zhang B 2020 Probing the Performance of Structurally Controlled Platinum-Cobalt Bimetallic Catalysts for Selective Hydrogenation of Cinnamaldehyde *J. Catal.* **388** 164-70

[18] Hu Q, Wang S, Gao Z, Li Y, Zhang Q, Xiang Q and Qin Y 2017 The Precise Decoration of Pt Nanoparticles with Fe Oxide by Atomic Layer Deposition for the Selective Hydrogenation of Cinnamaldehyde *Appl. Catal. B* **218** 591-9

[19] Liu H, Chang L, Chen L and Li Y 2016 Nanocomposites of Platinum/Metal-Organic Frameworks Coated with Metal-Organic Frameworks with Remarkably Enhanced Chemoselectivity for Cinnamaldehyde Hydrogenation *ChemCatChem* **8** 946-51

[20] Gu Y, Zhao Y, Wu P, Yang B, Yang N and Zhu Y 2016 Bimetallic $Pt_xCo_y$ Nanoparticles with Curved Faces for Highly Efficient Hydrogenation of Cinnamaldehyde *Nanoscale* **8** 10896-901

[21] Wang X, He Y, Liu Y, Park J and Liang X 2018 Atomic Layer Deposited Pt-Co Bimetallic Catalysts for Selective Hydrogenation of α, β-Unsaturated Aldehydes to Unsaturated Alcohols *J. Catal.* **366** 61-9

[22] Wang K, Wang X and Liang X 2020 Synthesis of High Metal Loading Single Atom Catalysts and Exploration of the Active Center Structure *ChemCatChem* **13** 28-58

[23] Ji X, Niu X, Li B, Han Q, Yuan F, Zaera F, Zhu Y and Fu H 2014 Selective Hydrogenation of Cinnamaldehyde to Cinnamal Alcohol over Platinum/Graphene Catalysts *ChemCatChem* **6** 3246-53

[24] Shi W, Wu K-H, Xu J, Zhang Q, Zhang B and Su D S 2017 Enhanced Stability of Immobilized Platinum Nanoparticles through Nitrogen Heteroatoms on Doped Carbon Supports *Chem. Mater.* **29** 8670-8

[25] Wang H, Bai S, Pi Y, Shao Q, Tan Y and Huang X 2018 A Strongly Coupled Ultrasmall $Pt_3Co$ Nanoparticle-Ultrathin $Co(OH)_2$ Nanosheet Architecture Enhances Selective Hydrogenation of α,β-Unsaturated Aldehydes *ACS Catal.* **9** 154-9

[26] Wang X, Hu W, Deng B and Liang X 2017 Selective Hydrogenation of Citral over Supported Pt Catalysts: Insight into Support Effects *J. Nanoparticle Res.* **19** 153-63

[27] Shang H, Chen W, Jiang Z, Zhou D and Zhang J 2020 Atomic-Dispersed Platinum Anchored on Porous Alumina Sheets as an Efficient Catalyst for Diboration of Alkynes *Chem. Commun.* **56** 3127-30

[28] Taylor M J, Beaumont S K, Islam M J, Tsatsos S, Parlett C A M, Issacs M A and Kyriakou G 2021 Atom Efficient PtCu Bimetallic Catalysts and Ultra Dilute Alloys for the Selective Hydrogenation of Furfural *Appl. Catal. B* **284** 119737-46

[29] Cao L, Liu W, Luo Q, Yin R, Wang B, Weissenrieder J, Soldemo M, Yan H, Lin Y, Sun Z, Ma C, Zhang W, Chen S, Wang H, Guan Q, Yao T, Wei S, Yang J and Lu J 2019 Atomically Dispersed Iron Hydroxide Anchored on Pt for Preferential Oxidation of CO in $H_2$ *Nature* **565** 631-5

[30] Knez M, Nielsch K and Niinistö L 2007 Synthesis and Surface Engineering of Complex Nanostructures by Atomic Layer Deposition *Adv. Mater.* **19** 3425-38

[31] Lee H-B-R and Bent S F 2011 Microstructure-Dependent Nucleation in Atomic Layer Deposition of Pt on $TiO_2$ *Chem. Mater.* **24** 279-86

[32] Zhang J, Zheng X, Yu W, Feng X and Qin Y 2022 Unravelling the Synergy in Platinum-Nnickel Bimetal Catalysts Designed by Atomic Layer Deposition for Efficient Hydrolytic Dehydrogenation of Ammonia Borane *Appl. Catal. B.* **306** 121116
[33] Díaz-López J A, Guilera J, Biset-Peiró M, Enache D, Kelly G and Andreu T 2021 Passivation of $Co/Al_2O_3$ Catalyst by Atomic Layer Deposition to Reduce Deactivation in the Fischer–Tropsch Synthesis *Catalysts* **11**
[34] Bai S, Huang B, Shao Q and Huang X 2018 Universal Strategy for Ultrathin Pt-M (M = Fe, Co, Ni) Nanowires for Efficient Catalytic Hydrogen Generation *ACS Appl. Mater. Interfaces* **10** 22257-63
[35] Aricò A S, Shukla A K, Kim H, Park S, Min M and Antonucci V 2001 An XPS Study on Oxidation States of Pt and Its Alloys with Co and Cr and Its Relevance to Electroreduction of Oxygen *Appl. Surf. Sci.* **172** 33-40
[36] Xia B Y, Wu H B, Li N, Yan Y, Lou X W D and Wang X 2015 One-Pot Synthesis of Pt-Co Alloy Nanowire Assemblies with Tunable Composition and Enhanced Electrocatalytic Properties *Angew. Chem. Int. Ed.* **127** 3868-72
[37] Cao M, Wu D and Cao R 2014 Recent Advances in the Stabilization of Platinum Electrocatalysts for Fuel-Cell Reactions *ChemCatChem* **6** 26-45
[38] He S, Xie L, Che M, Chan H C, Yang L, Shi Z, Tang Y and Gao Q 2016 Chemoselective Hydrogenation of α,β-Unsaturated Aldehydes on Hydrogenated MoOx Nanorods Supported Iridium Nanoparticles *J. Mol. Catal. A* **425** 248-54
[39] Xu D, Wu B, Ren P, Wang S, Huo C, Zhang B, Guo W, Huang L, Wen X, Qin Y, Yang Y and Li Y 2017 Controllable Deposition of Pt Nanoparticles into a KL Zeolite by Atomic Layer Deposition for Highly Efficient Reforming of n-Heptane to Aromatics *Catal. Sci. Technol.* **7** 1342-50
[40] Nabaho D, Niemantsverdriet J W, Claeys M and van Steen E 2016 Hydrogen Spillover in the Fischer–Tropsch Synthesis: An Analysis of Platinum as a Promoter for Cobalt–Alumina Catalysts *Catal. Today* **261** 17-27
[41] Reynoso A J, Ayastuy J L, Iriarte-Velasco U and Gutiérrez-Ortiz M Á 2020 Bimetallic Pt-Co Catalysts for the Liquid-Phase WGS *Catalysts* **10** 830-50
[42] Reynoso A J, Ayastuy J L, Iriarte-Velasco U and Gutiérrez-Ortiz M A 2018 Cobalt Aluminate Spinel-Derived Catalysts for Glycerol Aqueous Phase Reforming *Appl. Catal. B.* **239** 86-101
[43] Durndell L J, Parlett C M, Hondow N S, Isaacs M A, Wilson K and Lee A F 2015 Selectivity Control in Pt-Catalyzed Cinnamaldehyde Hydrogenation *Sci. Rep.* **5** 9425
[44] Breen J 2004 Steric Effects in the Selective Hydrogenation of Cinnamaldehyde to Cinnamyl Alcohol using an Ir/C Catalyst *Appl. Catal. A* **268** 267-74
[45] Oduro W O, Cailuo N, Yu K M, Yang H and Tsang S C 2011 Geometric and Electronic Effects on Hydrogenation of Cinnamaldehyde over Unsupported Pt-based Nanocrystals *Phys. Chem. Chem. Phys.* **13** 2590-602
[46] Schettino V and Bini R 2007 Constraining Molecules at the Closest Approach: Chemistry at High Pressure *Chem. Soc. Rev.* **36** 869-80
[47] Lv Y, Han M, Gong W, Wang D, Chen C, Wang G, Zhang H and Zhao H 2020 Fe-Co Alloyed Nanoparticles Catalyzing Efficient Hydrogenation of Cinnamaldehyde to Cinnamyl Alcohol in Water *Angew. Chem. Int. Ed.* **59** 23521-6

[48] Xin H, Zhang W, Xiao X, Chen L, Wu P and Li X 2021 Selective Hydrogenation of Cinnamaldehyde with $Ni_xFe_{1-x}Al_2O_{4+\delta}$ Composite Oxides Supported Pt Catalysts: C=O versus C=C Selectivity Switch by Varying the Ni/Fe Molar Ratios *J. Catal.* **393** 126-39

[49] Cao Z, Bu J, Zhong Z, Sun C, Zhang Q, Wang J, Chen S and Xie X 2019 Selective Hydrogenation of Cinnamaldehyde to Cinnamyl Alcohol over BN-Supported Pt Catalysts at Room Temperature *Appl. Catal. A* **578** 105-15

[50] Delbecq F and Sautet P 1995 Competitive C=C and C=O Adsorption of α-β-Unsaturated Aldehydes on Pt and Pd Surfaces in Relation with the Selectivity of Hydrogenation Reactions: A Theoretical Approach *J. Catal.* **152** 217-36

[51] Li Y, Lai G-H and Zhou R-X 2007 Carbon Nanotubes Supported Pt–Ni Catalysts and Their Properties for the Liquid Phase Hydrogenation of Cinnamaldehyde to Hydrocinnamaldehyde *Appl. Surf. Sci.* **253** 4978-84

[52] Tsang S C, Cailuo N, Oduro W, Kong A T, Clifton L, Yu K M, Thiebaut B, Cookson J and Bishop P 2008 Engineering Preformed Cobalt-Doped Platinum Nanocatalysts for Ultraselective Hydrogenation *ACS Nano* **2** 2547-53

[53] Pan H, Li J, Lu J, Wang G, Xie W, Wu P and Li X 2017 Selective Hydrogenation of Cinnamaldehyde with $PtFe/Al_2O_3$@SBA-15 Catalyst: Enhancement in Activity and Selectivity to Unsaturated Alcohol by Pt-FeO and Pt-$Al_2O_3$@SBA-15 Interaction *J. Catal.* **354** 24-36

# Supporting Information

## Highly stable Pt-Co bimetallic catalysts prepared by atomic layer deposition for cinnamaldehyde selective hydrogenation

Kaiying Wang [a], Xiaoqing He [b,c], Jee-Ching Wang [a], Xinhua Liang [a,*]

[a] Linda and Bipin Doshi Department of Chemical and Biochemical Engineering, Missouri University of Science and Technology, Rolla, Missouri 65409, United States

[b] Electron Microscopy Core Facility, University of Missouri, Columbia, Missouri 65211, United States

[c] Department of Mechanical and Aerospace Engineering, University of Missouri, Columbia, Missouri 65211, United States

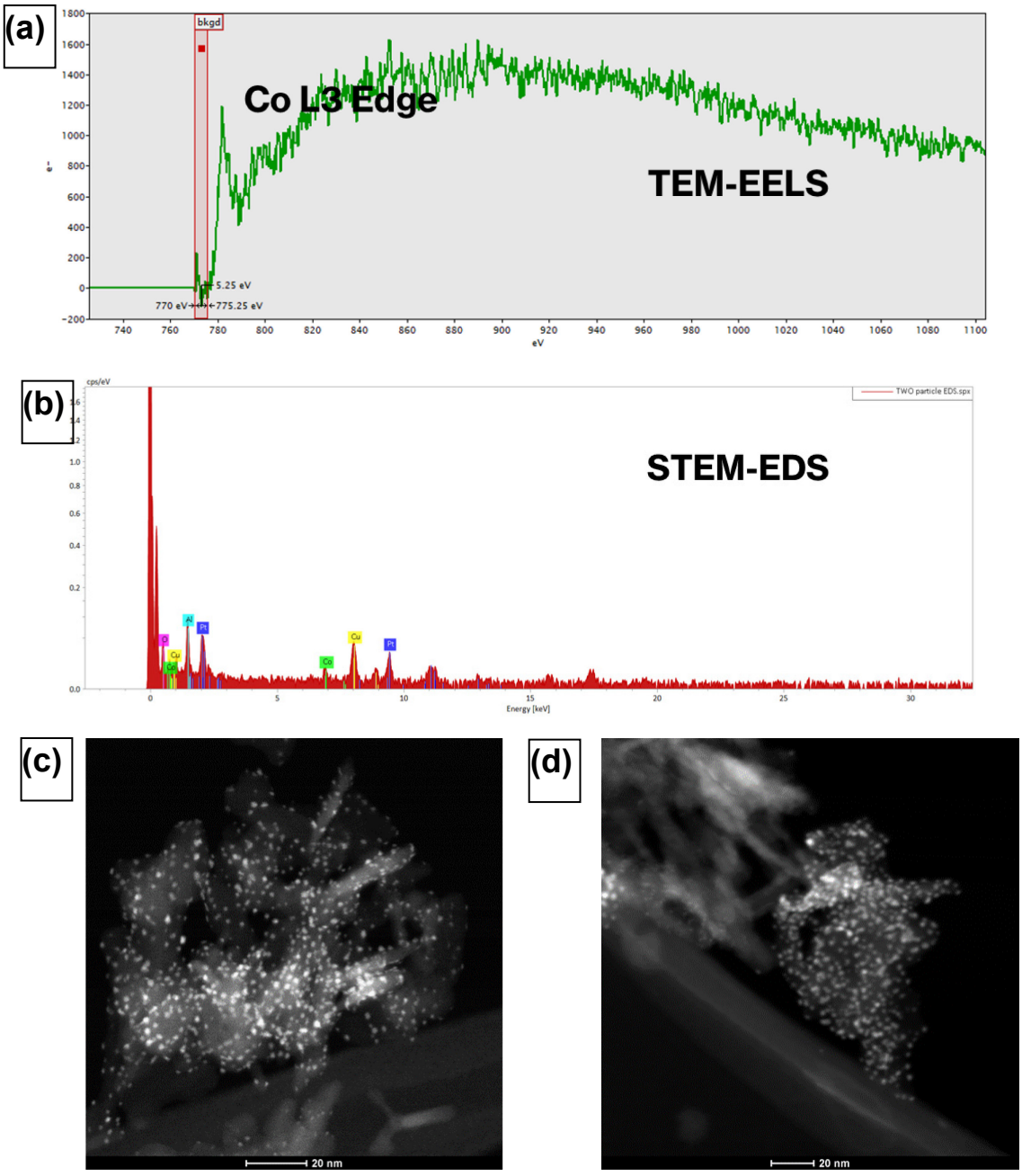


**Fig. S1** (a) TEM-EESL and (b) STEM-EDS spectra of 5cCo2cPt sample. High angle annular dark field images of (c) 2cPt and (d) 5cCo2cPt samples.

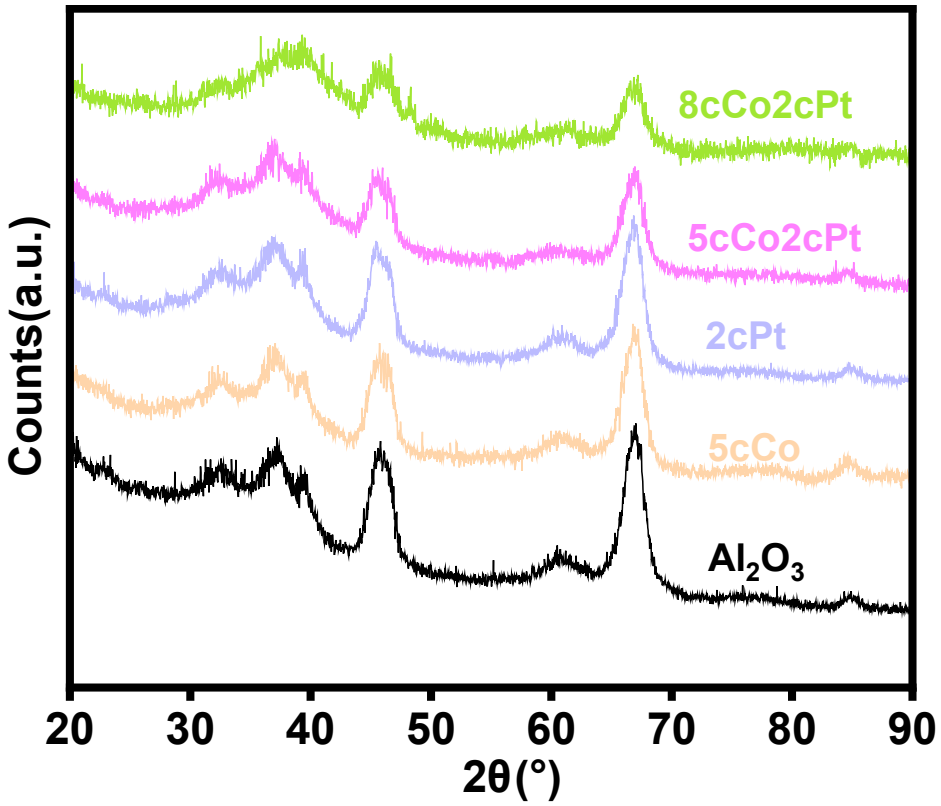


**Fig. S2** XRD patterns of the obtained samples.

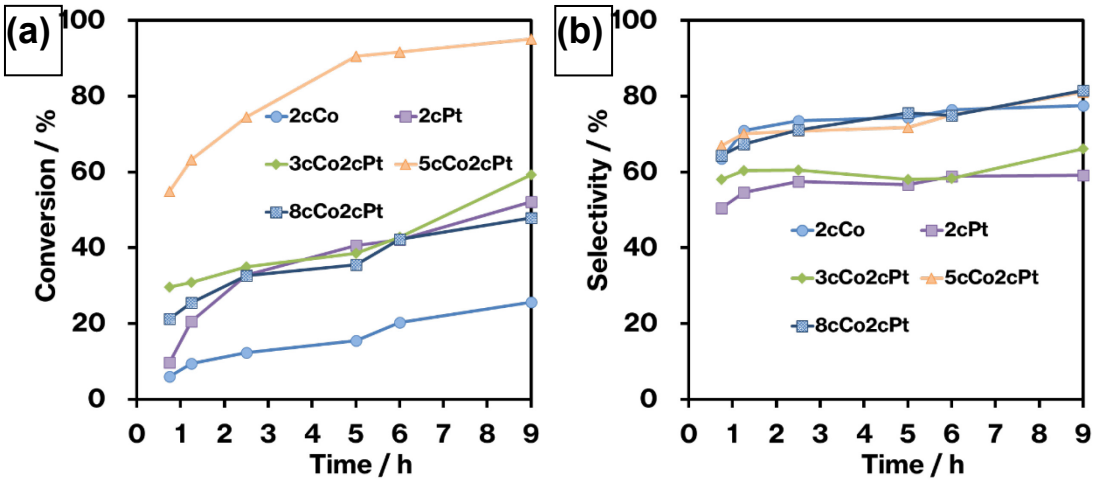


**Fig. S3** Effects of Pt/Co ratios on (a) CAL conversion and (b) selectivity.

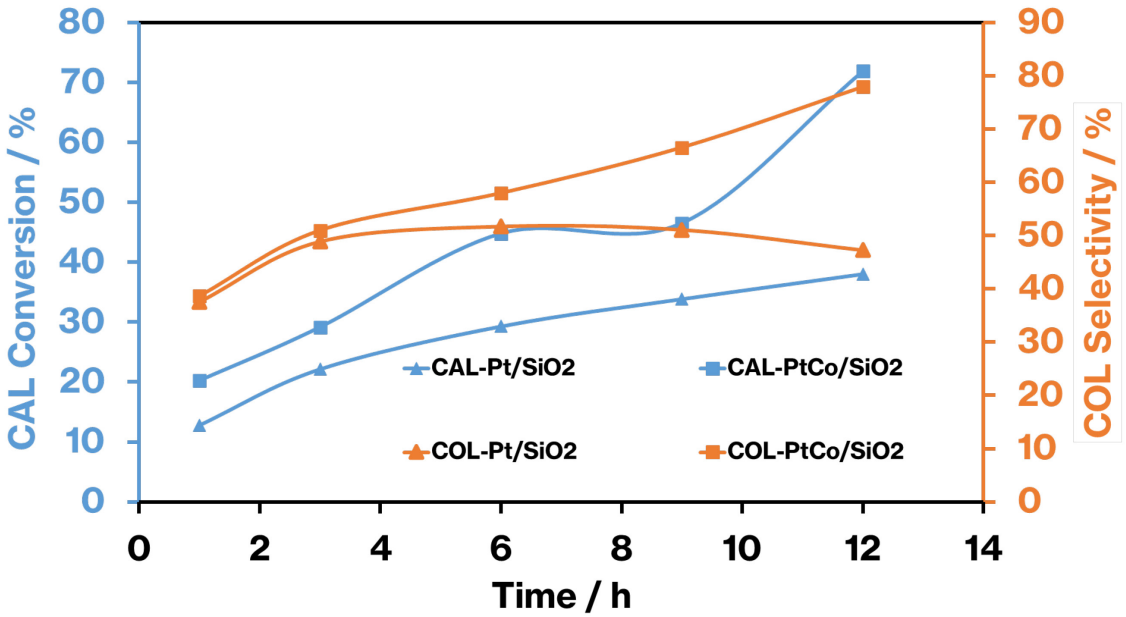


**Fig. S4** CAL conversion and COL selectivity over $Pt/SiO_2$ and $PtCo/SiO_2$ catalysts.